Water splitting into hydrogen and oxygen by non-traditional redox inactive zinc selenolate electrocatalyst

Aditya Upadhyay
Indian Institute of Science Education and Research Bhopal
Saurav KV
Indian Institute of Science Education and Research Bhopal
Manish Kumar
Indian Institute of Science Education and Research Bhopal
Evelin Varghese
Indian Institute of Science Education and Research Bhopal
Ananda Hodage
Indian Institute of Science Education and Research Bhopal
Amit Paul
Indian Institute of Science Education and Research Bhopal
Srinivasan
Indian Institute of Science Education and Research, Bhopal
Sangit Kumar (sangitkumar@iiserb.ac.in)
Indian Institute of Science Education and Research Bhopal https://orcid.org/0000-0003-0658-8709

Article

Keywords: water splitting, non-traditional redox inactive zinc selenolate electrocatalyst

Posted Date: September 24th, 2020

DOI: https://doi.org/10.21203/rs.3.rs-77259/v1

Abstract

The development of alternative energy sources is the utmost priority of the developing society. Unlike many prior homogenous electrocatalysts that rely on the change in an oxidation state of metal center and or electrochemically active ligand, the synthesized novel bimetallic zinc selenolate complex consisting of redox inactive zinc metal ion and catalytically inactive ligand catalyzes the electrochemical oxygen evolution from the water with rate constant 7.28 s-1 at onset potential 1.028 V vs. NHE. On the other hand, the hydrogen evolution reaction proceeds with 47.32 s-1 observed rate constant and -0.256 V onset potential vs. NHE. DFT computations and control experiments suggest that the redox chemistry at selenium center, Lewis acidity, and cooperativity effect of two zinc atoms facilitate the electrochemical oxidation and reduction of water into oxygen and hydrogen, respectively.

Introduction

With the exponential increase in the consumption of current energy sources across the world, the biggest challenge that lies ahead is the development of alternative energy sources that are competitive with the currently available energy resources.[1] Over the past decades, substantial progress has been made in energy production electrochemically, mainly those involving water, hydrogen, and oxygen, wherein water oxidizes at the anode, known as oxygen evolution reaction (OER) and the reduction of the proton to the hydrogen, termed as hydrogen evolution reaction (HER) occurs at the cathode.[2-4] Generally, heavy transition metal (TM) catalytic system augment OER and HER.[5-12] In these catalysts, the metal ion performs the electron transfer and also interacts with the substrate during bond-forming and breaking events.[13-14] Consequently, a metal center is associated with the formation of metal hydride and metal oxide intermediates in HER and OER, respectively. Moreover, earth-abundant 3d-transition metals such as nickel, copper, and cobalt complexes (Scheme 1) have been prepared with the appropriate choice of organosulfur and organoselenium ligands having selenium or sulfur at the active site to interact with the proton and to assist the formation of a metal-hydride bond by the proton shuttling process, which is the crucial step in the reduction of proton in hydrogen evolution reaction.[15-20] Besides the organotransition metal selenolate electrocatalysts, the selenium and transition metals (Fe, Co, Ni, Cu) derived materials also provide an alternate for the electrocatalytic water oxidation and water reduction reactions (OER and HER).[21]

Further, for oxygen evolution reaction (OER) from water, redox active ligands have been employed to stabilize the high oxidation state of central 3d-transition metal in the catalytic intermediates which enhances the reactivity of the oxidized metal oxide intermediates.[22-27] Thus, the reactivity of metal-hydride and metal oxide bonds is crucial for optimum catalytic efficiency. Also, the traditional metal hydrides and metal oxides require open coordination sites and able to accommodate multiple redox two and four-electron processes.[28-29]

In this context, it is desirable to explore new pathways in which metal hydrides are not necessary to involve in the catalytic cycle. Further, economic and sustainable alternatives are highly desirable to ease out the dependency on the transition metals (TMs, *vide infra*). In 2016, Graupperhaus and co-workers reported the electrocatalytic proton reduction of acetic acid and oxidation of hydrogen gas by redox-active thiosemicarbazone ligand along with its zinc complex by avoiding the traditional metal hydride approach (Scheme 1).[30-31] Nonetheless, zinc complexes have not been reported, which could electrocatalyze water splitting. Sun *et al*. have unsuccessfully attempted the electrocatalytic water reduction by using zinc(II)pentapyridine complex. However, the cobalt(II) complex of the same ligand was successfully able to reduce water electrocatalytically.[32]

From the past decade, our group has been active in the synthesis and catalytic activity of organoselenium compounds.[33-35] Recently our group has reported a diorgano diselenide derived from the *o*-aminodiselenide ligand, which could activate aerial oxygen towards the oxidation of organothiols.[36-37] Inspired by nature[38] and by the non-transition metal electrocatalysts; zinc thiosemicarbazone and aluminium-bis aminopyridine (Scheme 1) for hydrogen evolution reactions (HER) from water,[30-31,39-40] herein, we report the synthesis and structural characterization of the novel bimetallic zinc selenolate electrocatalyst **1** that catalyzes the water-splitting reaction by ligand assisted pathways in both directions; oxygen evolution and hydrogen evolution reactions without adding acid or base. Mechanistic insights into the electrocatalytic activity of bimetallic zinc selenolate complex have also been gained by synthesizing mercury selenolate catalyst.

Results And Discussion

Electrochemical Studies

The cyclic voltammogram (CV) of catalyst **1** at 1 mM in propylene carbonate obtained using a glassy carbon electrode displayed a pronounced catalytic wave. Propylene carbonate solvent was chosen for the electrocatalysis because of it has wide potential window with an oxidative limit of >2.0 (*vs.* NHE), and weak coordinating ability in comparison with water.[7,50-51] The onset of the catalytic wave was observed at 1.13 V versus normal hydrogen electrode (NHE, the potentials presented in this study are referenced to it). The cyclic voltammogram of catalyst **1** revealed a one-electron oxidation wave at 1.14 V *vs.* NHE, corresponding to the oxidation of Se^{-2} to Se^{-1},[52] while a weak reverse peak was also observed (Figure 2A). A solution of bimetallic zinc catalyst **1** (1 mM) in propylene carbonate solution containing 1% water shows an increase in anodic current of 19 μA in comparison to without water (Figure 2A).

Further, the anodic current increases up to 31 μA with increasing water concentration in the electrochemical cell, which is indicative of an electrocatalytic OER process. The catalytic current remained unaltered beyond 4% of water, suggesting saturation of OER with a significant increase in the anodic current (ΔI = 16.42 μA) with k_{obs} = 7.28 s^{-1} (Figure S4, SI). However, the first oxidation wave remains unaltered during the electrocatalysis, implying the stability of the ligand during water oxidation

by catalyst **1**. Further, a decrease in the catalytic current was observed with an increase in the scan rate (Figure S5, SI), which indicates that the current is associated with the catalytic process.

The addition of water to the solution (1 mM) of diselenide **3**, which is a ligand for zinc selenolate catalyst **1**, increases the current by only ΔI = 0.12 μA (Figure S28, SI). Moreover, the addition of water does not enhance the current, which implies the inability of diselenide ligand **3** to catalyze water oxidation. Similarly, $ZnCl_2$ solution (1 mM) does not catalyze the water oxidation as no change in the anodic current was observed (Figure S29, SI), and instead, precipitation was observed in the electrochemical cell during the first cycle of electrocatalysis.

Next, we sought to study the hydrogen evolution reaction (HER) from water in propylene carbonate solution by using glassy carbon (GC) working electrode. For this, the electrochemical experiment was performed in the presence of 1 mM of catalyst **1** and 0.25% of water under cathodic (negative) potential. A successive increase of water in the cell results in an increase in the cathodic current (Figure 2C). The maximum cathodic current 12 μA (ΔI = 9 μA) was elevated at 1.5% water concentration. However, the onset potential of -0.256 V *vs.* NHE was observed along with rate constant (k_{obs}) of 47.32 s^{-1} (Figure S10, SI). Notably, the hydrogen evolution reaction (HER) from water in the presence of catalyst **1** under acidic conditions (using aqueous acetic acid and strong trifluoracetic acid, TFA) led to low cathodic current 14.8 μA (ΔI = 5.1 μA) and 3.2 μA (ΔI = 0.8 μA), (Figure S14 and S16, SI) contrary to the earlier reported catalysts in which addition an acid increases the cathodic current. It seems that the hydrogen evolution reaction (HER) catalyzed by zinc selenolate catalyst **1** proceeds preferentially by the deprotonation from water and may not from the acid, and significantly low rate constant in a strong trifluoroacetic acid could be due to the poor stability of the catalyst **1** in TFA.

To gain a deeper insight into the catalytic activity, the kinetic activities have been studied for OER and HER. A plot of i_{cat}/i_p *vs.* $[H_2O]^{1/2}$ was found to be linear, indicating bimolecular first-order reaction kinetics (Figure S4 and S10, SI). Similarly, a linear plot for i_{cat} *vs.* [catalyst **1**] was observed upon varying the concentration of zinc selenolate catalyst **1**, which suggests first-order reaction kinetics with respect to the catalyst **1** (Figures 2B and 2D).

The stability of zinc selenolate catalyst **1** under oxygen and hydrogen evolution reaction conditions is confirmed by constant potential electrolysis (CPE) at an applied potential of 1.34 V (*vs.* NHE for OER) and -0.26 V (*vs.* NHE for HER) for 2h at GC electrode surface in which a significant change in current was not observed (Figure 3A and 3B). Further, the stability of catalyst **1** under electrocatalysis was also confirmed by Electron Dispersive X-Ray Spectroscopy (EDXS) in which decomposition of catalyst **1** was not realized as a residue for Zn or zinc oxide/ zinc selenide was not observed in the spectra (Figure 3C, EDXS, blue part), and also scanning electron microscopy (SEM) study of Pt-electrode does not show any change in

the surface morphology (Figures 3C). The UV-Visible study was also performed on the solution from electrolysis cell after 2 h of the bulk electrolysis and before the electrolysis. The characteristic absorbance at 380 nm of zinc selenolate catalyst **1** was nearly identical (red and blue lines in Figure 3D) to the one before electrolysis (black line) confirms that the structure of the catalyst **1** remains unchanged after the electrocatalysis. These results demonstrate that the bimetallic zinc selenolate complex **1** serves as a robust catalyst for water splitting in a homogeneous system. Also, the evolved oxygen from the water during electrocatalysis was then determined by CPE, reveals a Faradic efficiency of 79% for oxygen evolution (Figure S22, SI).

Heavier analog mercury selenolate **4** also catalyzed oxygen evolution reaction (Figure, S23, SI), albeit low cathodic current 14 μA, and rate constant (0.038 s^{-1}) (Figure S24, SI), presumably attributed to monometallic nature, was observed in comparison to the bimetallic zinc selenolate catalyst **1**. Further, mercury selenolate **4** failed to catalyze the hydrogen evolution reaction (HER) from water (Figure S27). Mercury selenolate **4** was found unstable under negative potential as deposition was observed on the surface of the working electrode, presumably due to reduced mercury and could be due to feasible standard reduction potential (0.74V *vs*. SHE) of mercury ion to mercury than that of hydrogen ion to H_2.

Mechanistic Studies

Mechanistic insights on bimetallic zinc selenolate **1** catalyzed OER and HER from water were gained from the theoretical assessment of the likely reaction pathways supported by the mass analysis and control experiments. The free energies of intermediates along with possible HER and OER pathways, depicted in Scheme 3, were calculated at DFT/B3LYP/def2-TZVP level of theory.

Both reactions proceed via adsorption of two hydrogen-bonded water molecules, with one coordinating to Zn(a) and the other forming a hydrogen bond to bridging oxygen yielding **1a** (ΔG = 54.91 kcal mol^{-1}), the formation of which also confirmed by mass spectrometry (Figure S1, SI)**.** In OER, diaqua species **1a** undergoes proton-coupled electron transfer (PCET) to form **1b** (confirmed by mass spectrometry Figure S2, SI) with Zn(a)-OH and Zn(b)-OH_2 centers. Spin-density and NBO analysis (Figure S30, SI) indicates that the electron is lost primarily from Se(a), consistent with the Se^{-2}/Se^{-1} oxidation peak seen in the CV. A second PCET, accompanied by intramolecular rearrangements, leads to selenenic acid **1c**. Here selenium plays a crucial role in stabilizing the –OH bridging it to Zn(a), whereas the second –OH migrates to bridge the two Zn centers and bridging μ-phenolic oxygen become terminal. The next two successive PCET steps provide selenoxide species **1d** and the intramolecular ZnO---H(N) hydrogen-bonded intermediate **1e**, respectively. Poor stability of selenoxide (Se=O) bond attributed to weaker π-overlap of selenium with oxygen[53] and better leaving group tendency of selenium in the ligand[37,53] facilitate **1e** to undergo an intramolecular rearrangement to **1f** containing divalent selenium center and a peroxo linkage ($r_{O\text{-}O}$ = 1.48Å) between Zn centers and a phenolic ring. Subsequently, better ligation ability of water than oxygen to zinc would lead to oxygen evolution from **1f** with the concomitant release zinc selenolate catalyst **1a**.

The HER mechanism, also initiated by the formation of **1a**, proceeds with the abstraction of a proton from water by Se(a) to form **1g** under applied negative potential. Subsequently, H from –Se(a)H and –NH groups combine to evolve as H_2 yielding selone **1h**.[37] An added electron then reduces **1h** to the anion radical intermediate **1i** where the electronic charge on Se (0.24 e^-) and radical on N (0.33 e^-) are in conjugation through the phenyl ring (0.39 e^-) as confirmed using spin density (see inset of Scheme 3) and natural bond order (NBO) analysis. Next, the addition of water molecule and removal of OH^- anion effectively adds a proton to the system resulting in the radical intermediate **1m** stabilized by conjugation with the phenyl ring. Subsequently, the sequential addition of electron and proton regenerates the water adsorbed state **1a** (Scheme S3, SI).

Discussion

In summary, a novel bimetallic zinc selenolate has been synthesized and structurally characterized. Further, bimetallic zinc selenolate electrocatalyzed both OER and HER from water in without adding acid or base and could complement TM catalysts and redox-active ligands. The synthesized complex catalyzes the water splitting *via* ligand assisted pathway, which bypasses the formation of metal hydrides during catalysis. However, ligand and $ZnCl_2$ alone are not able to electrocatalyze the water splitting; only by combining these two show the catalytic activity where the Lewis acidity of Zn(II) plays a vital role in the mechanism as it binds with a water molecule and then would help in the removal of a proton from ligated water and also tune the redox potential of catalyst. From the mechanism, it is clear that the presence of a selenium center is crucial for the electrocatalysis of water. The reaction mainly occurs at the selenium center for the four-electron and two-electron transfer in oxygen evolution reaction (OER) and hydrogen evolution reaction (HER), respectively, while the Lewis acidic Zn(II) center brings the water molecule near to the active selenium center. Furthermore, we noted that the oxygen and nitrogen heteroatoms present in **1** is not only crucial for the isolation of bimetallic zinc complex but also facilitate electron transfer in OER and HER as this not only serve as two electrons donor and acceptor due to the presence of the *ortho*-amino group but also selenium seems weak electrophile and avoid forming an undesirable stable selenium-oxygen bond. It is also evident from our DFT analysis that selenium is a crucial active site on bimetallic zinc selenolate electrocatalyst for both OER and HER. Further progress is being made to enhance the reactivity of ligand in the bimetallic selenolate complexes to synergistically activate the small molecules, as we have presented here.

Methods

Representative Procedure. To the stirred solution of schiff base diselenide **2** (248 mg, 0.45 mmol, 1 equiv.) in ethanol, we added sodium borohydride (76 mg, 2.0 mmol, 4 equiv) to generated in-situ selenol and stirred the solution up to 4 h at room temperature. Then we added zinc chloride (122 mg, 0.9 mmol, 2 equiv.) and stirred the solution for 2 h. After that, the solvent was removed by the rotatory evaporator, and the solid residue was washed with aqueous sodium bicarbonate solution several times to afford a light

yellow colored novel bimetallic zinc selenolate complex **1** in (230 mg) 75% yield. Crystallization was done in DMSO water (2:1) mixture to afford yellow-colored crystals.

Electrochemistry. A potentiostat (SP-240 Bio-logic Instrument) was used for electrochemical measurements. The three-electrode electrochemical cell consisted of a Glassy carbon (3 mm Diameter) as the working electrode, a nonaqueous $Ag/AgNO_3$ (10 mM $AgNO_3$) as a reference electrode and a platinum wire as a counter electrode were used for the electrochemical measurements.

The electrochemical potential was converted relative to the normal hydrogen electrode (NHE; all potentials reported in this work are referenced to the NHE) following a literature protocol. Current and peak potentials for the catalytic waves were compared without addition of H_2O or TFA (i_p) and with the addition of H_2O or TFA (i_{cat}). Current ratios, i_{cat}/i_p, were plotted *vs.* $[H_2O]^{1/2}$ and $[TFA]^{1/2}$ to determine first-order rate constants (k) using the of Eq. 1 for OER and Eq. 2 for HER.

$$\frac{i_{cat}}{i_p} = \frac{(RT)^{1/2}}{0.446(nF\square)^{1/2}}(k_{cat})^{1/2}$$

1

$$\frac{i_{cat}}{i_p} = \frac{(RT)^{1/2}}{0.446(nF\square)^{1/2}}(k)^{1/2}\left(H_2O\right)^{1/2}$$

2

Wherein, *R*, *T*, *n*, *F*, and *v* are the universal gas constant, temperature, number of electrons transferred, Faraday constant, and scan rate, respectively.

The chronoamperometry experiment has been performed in a stirring electrolyte solution in order to make the solution free from in-situ generated oxygen bubbles. A potential of 1.34 V *vs.* NHE (for OER) and −0.26 V *vs.* NHE (for HER) has been chosen for the chronoamperometry experiment.

Computational Details. All the electronic structure calculations presented in this work were performed using density functional theory implemented in the TURBOMOLE 7.4 electronic structure package. Optimization of molecular geometry in the gas phase was carried out using B3LYP hybrid functional. The electronic configuration of the atoms was described with def2-TZVP basis set. For all the calculations, resolution of identity (RI) approximation with corresponding auxiliary basis set was used to speed up the calculations. The stability of the optimized geometries was confirmed by the absence of imaginary vibrational frequencies. Thermal corrections to Gibbs free energy, including zero-point energy, were obtained from vibrational frequency analysis at the same level of theory at 298.15 K and 1 atm within ideal-gas rigid-rotor harmonic-oscillator approximations.

Data availability. The authors declare that the data supporting the findings of this study are available within the paper and the Supplementary Information, as well as from the authors upon request.

Declarations

Author contributions

S.K. and A.U. designed the research. A.U., S.K.V. and E.V. performed the CV study and analyzed by A.P., A.H. and A.U. developed the methodology, M.K. and V.S. performed the theoretical studies, S.K., A.U., A.P., M.K. and V.S. wrote the manuscript.

Acknowledgments

SK acknowledges DST-SERB (CRG/2019/000017) New Delhi and IISER Bhopal for financial support. AUY and SKV (DST INSPIRE) acknowledges the IISER Bhopal for an Institute fellowship. Professor R. J Butcher (Howard University, Washington) for resolving the crystal structure of **1** (CCDC No. 194 9548). We sincerely thank the Department of Chemistry at IISER Bhopal for providing High-Performance Computing, Single Crystal XRD, and Scanning Electron Microscopy facilities.

References

1. Seh, W., Kibsgaard, J., Dickens, C. F., Chorkendorff, I., Nørskov J. K. & Jaramillo, T. F. Combining theory and experiment in electrocatalysis: Insights into materials design. *Science* **355**, 4998 (2017).
2. Li, J., Guttinger, R., More´, R., Song, F., Wan, W. & Patzke, G. R. Frontiers of water oxidation: The quest for true catalysts. *Soc. Rev.* **46**, 6124–6147 (2017).
3. Symes, M. D. & Cronin, L. Decoupling hydrogen and oxygen evolution during electrolytic water splitting using an electron-coupled-proton buffer. *Chem.* **5**, 403–409 (2013).
4. Wang, D., Sampaio, R. N., Troian-Gautier, L., Marquard, S. L., Farnum, B. H., Sherman, B. D., Sheridan, N. V., Dares, C. J., Meyer, G. J. & Meyer, T. J. Molecular photoelectrode for water oxidation inspired by photosystem II. *Am. Chem. Soc.* **141**, 7926–7933 (2019).
5. Hetterscheid, D. G. H., Van der Vlugt, J. I., Bruin, B. de. & Reek, J. N. H. Water splitting by cooperative catalysis. *Chem. Int. Ed.* **48**, 8178–8181 (2009)
6. Sala, X., Ertem, M. Z., Vigara, L., Todorova, T. K., Chen, W., Rocha, R. C., Aquilante, F., Cramer, C. J., Gagliardi, L. & Llobet, A. The cis-$[Ru^{II}(bpy)_2(H_2O)_2]^{2+}$ water oxidation catalyst revisited. *Angew Chem Int. Ed.* **49**, 7745–7747 (2010).
7. Chen, Z., Concepcion, J. J., Luo, H., Hull, J. F., Paul, A. & Meyer, T. J. Nonaqueous catalytic water oxidation. *Am. Chem. Soc.* **132**, 17670–17673 (2010).
8. Karunadasa, H. I., Chang, C. J. & Long, J. R. A molecular molybdenum-oxo catalyst for generating hydrogen from water. *Nature* **464**, 1329–1333 (2010).
9. Thoi, V. S., Sun, Y., Long, J. R. & Chang, C. J. Complexes of earth-abundant metals for catalytic electrochemical hydrogen generation under aqueous conditions. *Soc. Rev.* **42**, 2388–2400 (2013).

10. Norris, M. R., Concepcion, J. J., Fang, Z., Templeton, J. L. & Meyer, T. J. Low-overpotential water oxidation by a surface-bound ruthenium-chromophore–ruthenium-catalyst assembly. *Chem. Int. Ed.* **52**, 13580–13583 (2013).
11. Daniel, Q., Duan, L., Timmer, B. J. J., Chen, H., Luo, X., Ambre, R., Wang, Y., Zhang, B., Zhang, P., Wang, L., Li, F., Sun, J., Ahlquist, M. & Sun, L. Water oxidation initiated by in situ dimerization of the molecular Ru(pdc) catalyst *ACS Catal.* **8**, 4375–4382 (2018).
12. Matheu, R., Garrido-Barros, P., Gil-Sepulcre, Ertem, M. M. Z., Sala, X., Gimbert- Suriñach, C. & Llobet, A. The development of molecular water oxidation catalysts. *Rev. Chem.* **3**, 331–341 (2019).
13. Cao, R., Laia, W. & Du, P. Catalytic water oxidation at single metal sites. *Energy Environ. Sci.* **5**, 8134–8157 (2012).
14. Sundstrom, E. J., Yang, X., Thoi, V. S., Karunadasa, H. I., Chang, C. J., Long, J. R. & Head-Gordon, M. Computational and experimental study of the mechanism of hydrogen generation from water by a molecular molybdenum-oxo electrocatalyst. *Am. Chem. Soc.* **134**, 5233–5242 (2012).
15. Solis, B. H. & Hammes-Schiffer, S. Computational study of anomalous reduction potentials for hydrogen evolution catalyzed by cobalt dithiolene complexes. *Am. Chem. Soc.* **134**, 15253–15256 (2012).
16. Downes, C. A. & Marinescu, S. C. Efficient electrochemical and photoelectrochemical H_2 production from water by a cobalt dithiolene one-dimensional metal–organic surface**.** *Am. Chem. Soc.* **137**, 13740–13743 (2015).
17. Wombwell, C., Caputo, C. A. & Reisner, E. [NiFeSe]-Hydrogenase chemistry. *Chem. Res.* **48**, 2858–2865 (2015).
18. Downes, C. A. & Marinescu, S. C. Bioinspired metal selenolate polymers with tunable mechanistic pathways for efficient H_2 *ACS Catal.* **7**, 848–854 (2017).
19. Downes, C. A., Yoo, J. W., Orchanian, N. M., Haiges, R. & Marinescu, S. C. H_2 evolution by a cobalt selenolate electrocatalyst and related mechanistic studies. *Commun.* **53**, 7306–7309 (2017).
20. Koshiba, K., Yamauchi, K. & Sakai, K. A nickel dithiolate water reduction catalyst providing ligand-based proton-coupled electron-transfer pathways. *Chem. Int. Ed.* **56**, 4247 –4251 (2017).
21. Xia, X., Wang, L., Sui, N., Colvinc, V. L. & Yu, W. W. Recent progress in transition metal selenide electrocatalysts for water splitting. *Nanoscale* **12**, 12249–12262 (2020).
22. Su, X.-J., Zheng, C., Hu, Q.-Q., Du, H.-Y., Liao, R.-Z. & Zhang, M.-T. Bimetallic cooperative effect on O–O bond formation: Copper polypyridyl complexes as water oxidation catalyst. *Dalton Trans.* **47**, 8670-8675 (2018).
23. Du, H.-Y., Chen, S.-C., Su, X.-J., Jiao, L. & Zhang, M.-T. Redox-active ligand assisted multielectron catalysis: A case of CoIII complex as water oxidation catalyst. *Am. Chem. Soc.* **140**, 1557–1565 (2018).
24. Baydoun, H., Burdick, J., Thapa, B., Wickramasinghe, L., Li, D., Niklas, J., Poluektov, O. G., Schlegel, H. B. & Verani, C. N. Immobilization of an amphiphilic molecular cobalt catalyst on carbon black for

ligand-assisted Water Oxidation. *Chem.* **57**, 9748–9756 (2018).

25. Wang, D. & Groves, J. T. Efficient water oxidation catalyzed by homogeneous cationic cobalt porphyrins with critical roles for the buffer base. *Natl. Acad. Sci. U.S.A.* **110**, 15579–15584 (2013).
26. Nakazono, T., Parentab, A. R. & Sakai, K. Cobalt porphyrins as homogeneous catalysts for water oxidation. *Commun.* **49**, 6325–6327 (2013).
27. Wang, H.-Y., Mijangos, E., Ott, S. & Thapper, A. Water oxidation catalyzed by a dinuclear cobalt–polypyridine complex. *Chem. Int. Ed.* **53**, 14499 –14502 (2014).
28. Blakemore, J. D., Crabtree, R. H. & Brudvig, G. W. Molecular catalysts for water oxidation. *Rev.* **23**, 12974–13005 (2015).
29. Luo, G.-G., Zhang, H.-L., Tao, Y.-W., Wu, Q.-Y., Tianc, D. & Zhang, Q. Recent progress in ligand-centered homogeneous electrocatalysts for hydrogen evolution reaction. *Chem. Front.* **6**, 343–354 (2019).
30. Haddad, A. Z., Garabato, B. D., Kozlowski, P. M., Buchanan, R. M. & Grapperhaus, C. A. Beyond metal-hydrides: Non-transition-metal and metal-free ligand-centered electrocatalytic hydrogen evolution and hydrogen oxidation. *Am. Chem. Soc.* **138**, 7844–7847 (2016).
31. Cronin, S. P., Mamun, A. A., Toda, M. J., Mashuta, M. S., Losovyj, Y., Kozlowski, P. M., Buchanan, R. M. & Grapperhaus, C. A. Utilizing charge effects and minimizing intramolecular proton rearrangement to improve the overpotential of a thiosemicarbazonato zinc HER catalyst. *Chem.* **58**, 12986–12997 (2019).
32. Sun, Y., Bigi, J. P., Piro, N. A., Tang, M. L., Long, J. R. & Chang, C. J. Molecular cobalt pentapyridine catalysts for generating hydrogen from water. *Am. Chem. Soc.* **133**, 9212–9215 (2011).
33. Verma, A., Jana, S., Prasad, C. D., Yadav, A. & Kumar, S. Organoselenium and DMAP co-catalysis: Regioselective synthesis of medium-sized halolactones and bromooxepanes from unactivated alkenes. *Commun.* **52**, 4179–4182 (2016).
34. Kumar, S., Yan, J., Poon, J.-f., Singh, V. P., Lu, X., Ott, M. K., Engman, L. & Kumar, S. Multifunctional antioxidants-regenerable radical-trapping and hydroperoxide decomposing ebselenols. *Chem. Int. Ed.* **55**, 3729–3733 (2016).
35. Jana, S., Verma, A., Kadu, R. & Kumar, S. Visible-light-induced oxidant and metal-free dehydrogenative cascade trifluoromethylation and oxidation of 1,6-enynes with water. *Sci.* **8**, 6633–6644 (2017).
36. Balkrishna, S. J., Bhakuni, B. S. & Kumar, S. Copper catalyzed/mediated synthetic methodology for ebselen and related isoselenazolones. *Tetrahedron* **67**, 9565–9575 (2011).
37. Rathore, V., Upadhyay, A. & Kumar, S. A organodiselenide with dual mimic function of sulfhydryl oxidases and glutathione peroxidases: Aerial oxidation of organothiols to organodisulfides. *Lett.* **20**, 6274–6278 (2018).
38. Cox, N., Pantazis, D. A., Neese, F. & Lubitz, W. Artificial photosynthesis: understanding water splitting in nature. *Interface Focus* **5** (2015).

39. Qi, S., Fan, Y., Wang, J., Song, X., Li, W. & Zhao, M. Metal-free highly efficient photocatalysts for overall water splitting: C_3N_5 *Nanoscale* **12**, 306–315 (2020).
40. Thompson, E. J. & Berben, L. A. Electrocatalytic hydrogen production by an aluminum(III) complex: Ligand-based protonand electron transfer. *Chem. Int. Ed.* **54**, 11642–11646 (2015).
41. Cheng, Y., Emge T. J. & Brennan, J. G. Polymeric Cd(Se-2-NC_5H_4)2 and square planar Hg(Se-2-$NC_5H_4)_2$: Volatile CVD precursors to II-VI semiconductors *Chem.* **33**, 3711–3714 (1994).
42. Mugesh, G., Singh, H. B., Patel, R. P. & Butcher, R. J. Synthesis and structural characterization of monomeric selenolato complexes of zinc, cadmium, and mercury. *Chem.* **37**, 2663–2669 (1998).
43. Freedman, D., Kornienko, A., Emge, T. J. & Brennan, J. G. Divalent samarium compounds with heavier chalcogenolate (EPh; E = Se, Te) ligands. *Chem.* **39**, 2168–2171 (2000).
44. Ritch, J. S. & Chivers, T. Coordination chemistry of a new *P*,*Te*-centred ligand: synthesis, NMR spectra and X-ray structures of M(TePPr$^i_2$NPPr$^i_2)_2$ (M = Zn, Cd, Hg). *Dalton Trans.* 957–962 (2008).
45. Emge, T. J., Romanelli, M. D., Moore, B. F. & Brennan, J.G. Zinc, cadmium, and mercury complexes with fluorinated selenolate ligands. *Chem.* **49**, 7304–7312 (2010).
46. Pöllnitz, A., Silvestru, C., Carpentierb, J.-F. & Silvestru, A. Diorganodiselenides and zinc(II) organoselenolates containing (imino)aryl groups of type 2-(RN=CH)C_6H_4. *Dalton Trans.* **41**, 5060–5070 (2012,).
47. Sharma, R. K., Wadewala, A., Kedarnath, G., Vishwanadh, B. & Jain, V. K. Pyrimidyl-2-selenolates of cadmium and mercury: Synthesis, characterization, structures and their conversion to metal selenide nano-particles. *Chim. Acta* **411**, 90–96 (2014).
48. Patel, S., Meenakshi, Hodage, A. S., Verma, A., Agrawal, S., Yadav, A. & Kumar, S. Synthesis and structural characterization of monomeric mercury (II) selenolate complexes derived from 2-phenylbenzamide ligands. *Dalton Trans.* **45**, 4030–4040 (2016).
49. Byer, O., Lazebnik, B. F. & Smeltzer, D. L. *Methods for Euclidean Geometry*, Mathematical Association of America, Vol.**37**, pp. 51–52 (2010).
50. Coggins, M. K., Zhang, M-T, Vannucci, A. K., Dares, C. J. & Meyer, T. J. *Am. Chem. Soc.* **136**, 5531−5534 (2014).
51. Gagliardi, C. J., Vannucci, A. K., Concepcion, J. J., Chen, Z. & Meyer, T. J. *Energy Environ. Sci.* **5**, 7704–7717 (2012).
52. Engman, L., Perssorn, J., Andersson, C. M. & Berglund, M. Application of the hammett equation to the electrochemical oxidation of diaryl chalcogenides and aryl methyl chalcogenides. *Chem. Soc., Perkin Trans. 2*, 1309–1313 (1992).
53. Reich, H. J. & Hondal, R. J. Why nature chose selenium. *ACS Chem. Biol.* **11**, 821–841 (2016).

Figures

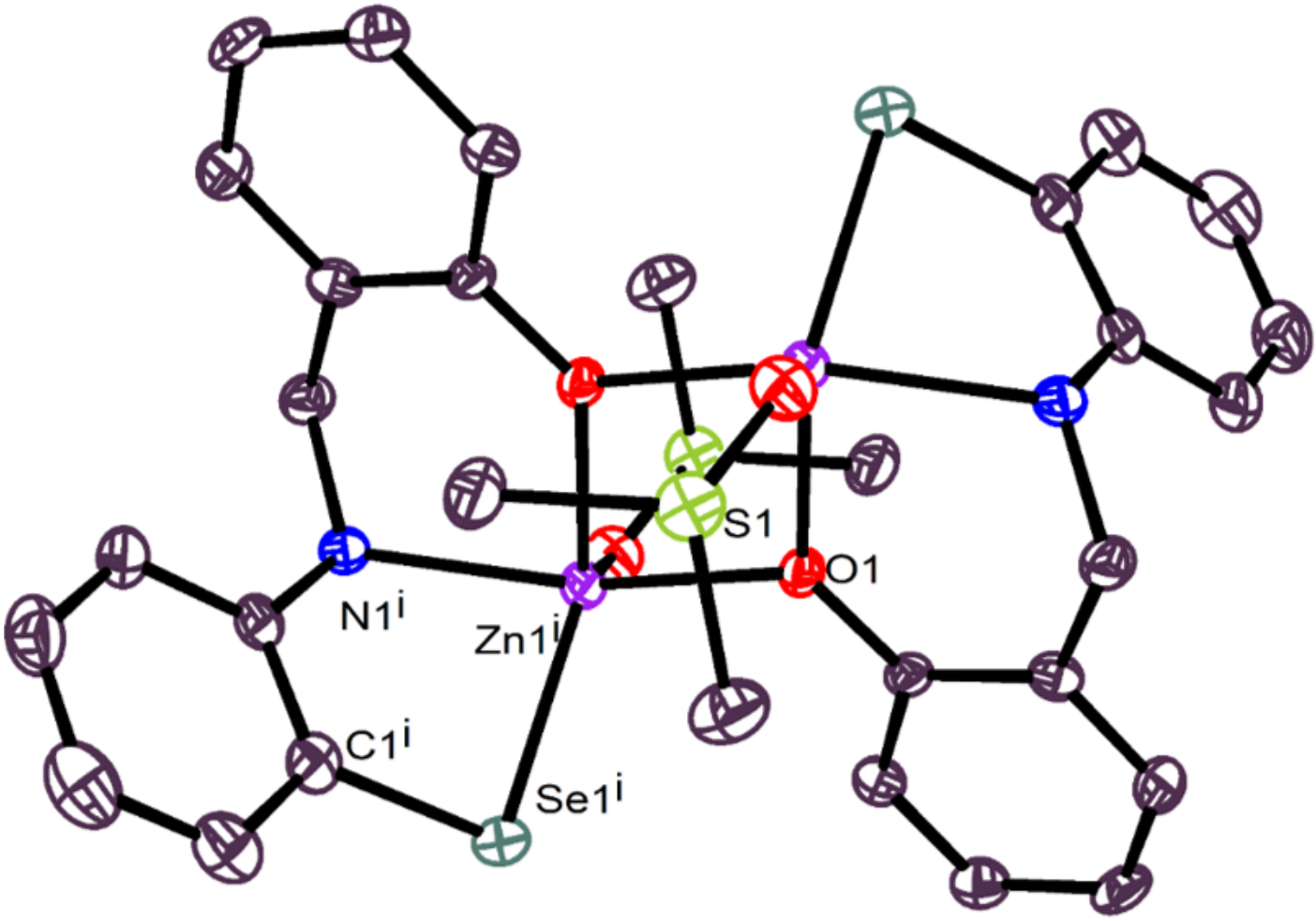

Figure 1

ORTEP view of bimetallic zinc selenolate complex 1 (ORTEP view of 1 with 50% thermal ellipsoid probability)

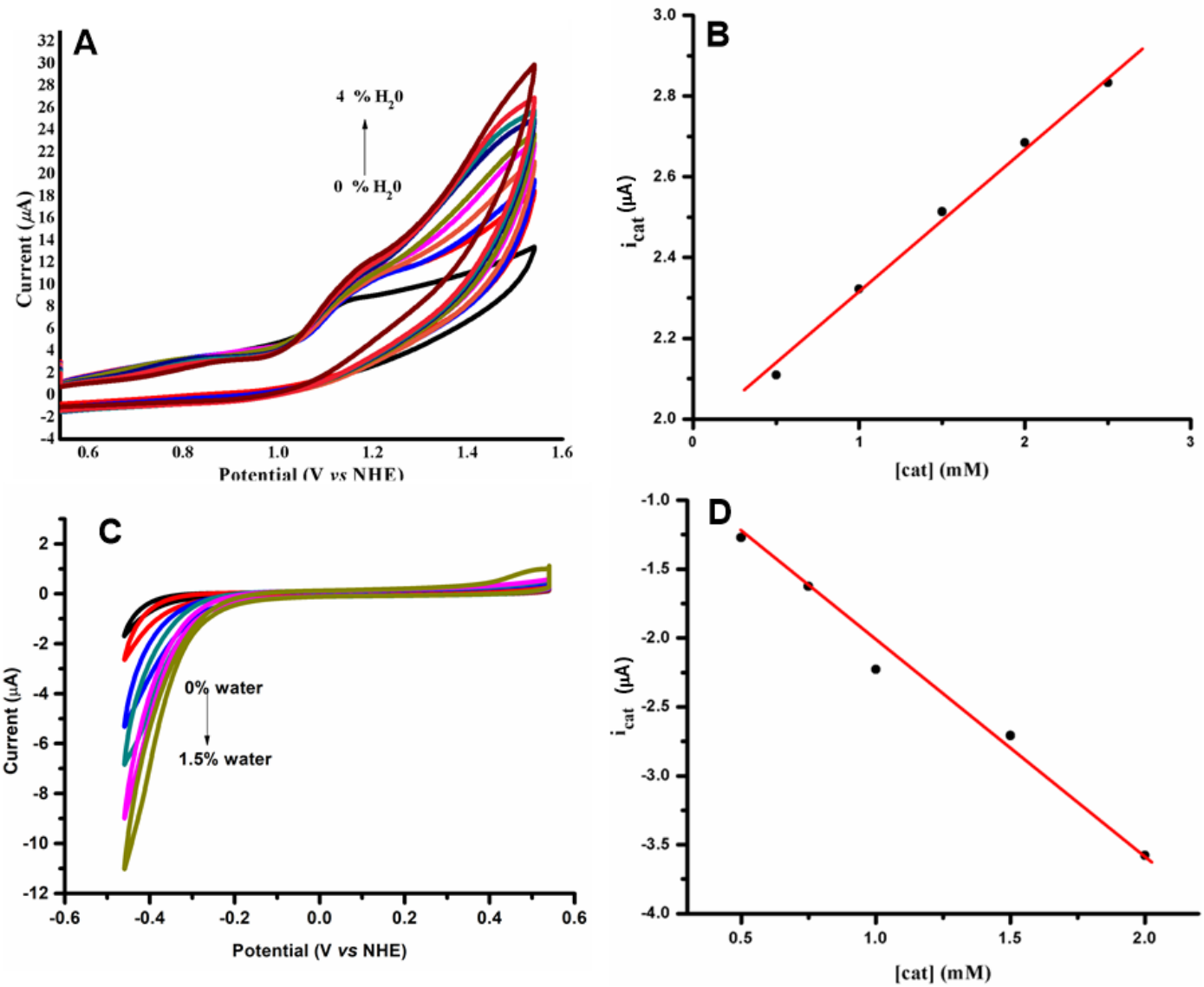

Figure 2

Electrochemical O2 and H2 evolution (A) OER with the addition of water (no water, 0.5%, 1%, 1.25%, 1.5%, 1.75%, 2%, 2.5%, 3%, 4%). (B) Linear plot of icat vs. [cat] in cathodic direction at 20mV/s scan rate. (C). HER with the addition of water (no water, 0.25%, 0.5%, 1.5%, 1.25%, 1.50%), by catalyst 1 (1 mM) using nBu4NPF6 as a supporting electrolyte in propylene carbonate solution. (D) Linear plot of icat vs. [cat] in anodic direction at 20 mV/s scan rate.

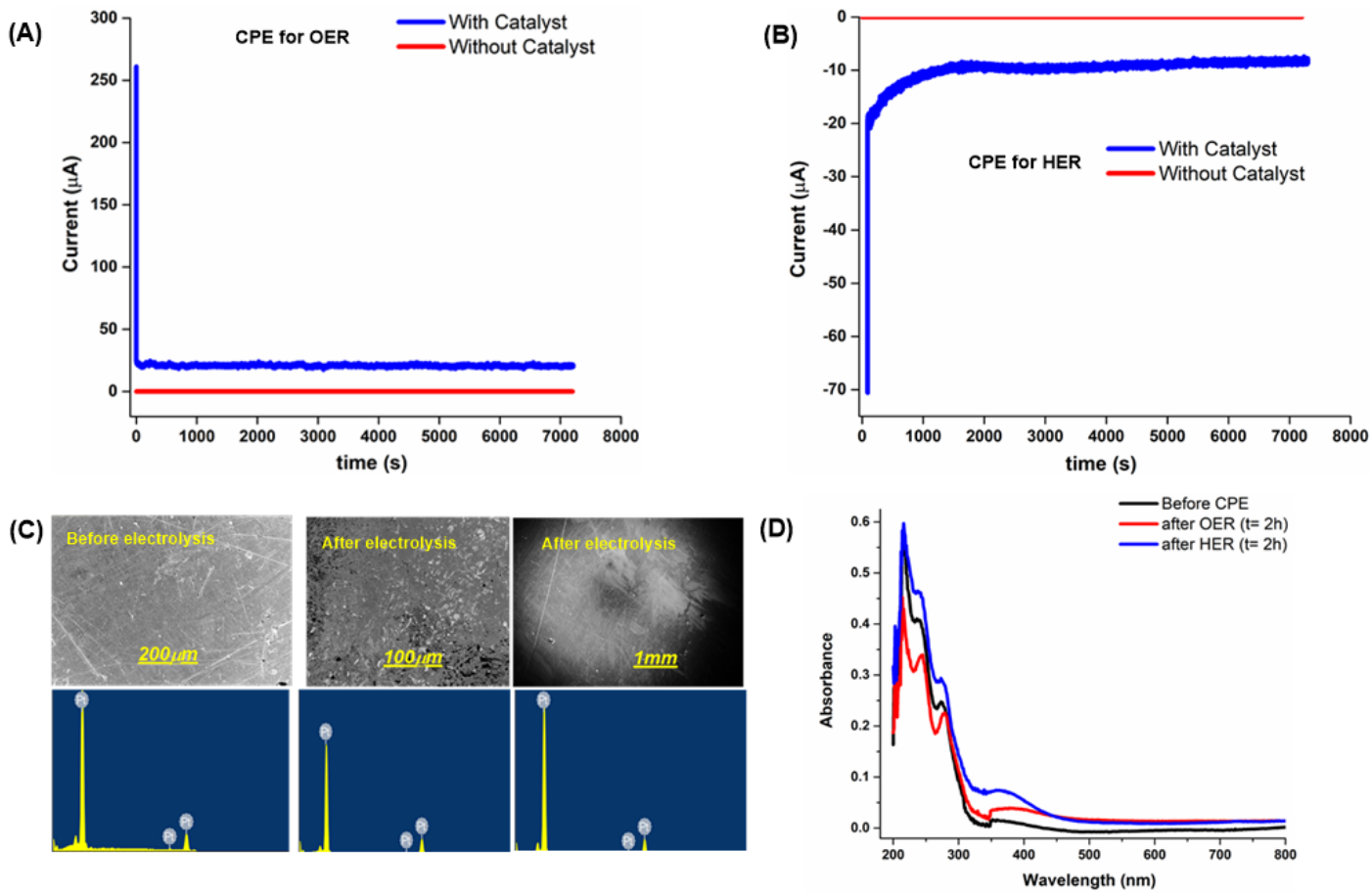

Figure 3

(A) and (B) Constant potential electrolysis for OER for 2 h at 1.34 V (for OER) and -0.26V (for HER). vs. NHE of catalyst 1 (5mM) using 0.1M nBu4NPF6 as supporting electrolyte in propylene carbonate solution. (C) SEM and EDXS images of Pt surface after constant potential electrocatalysis for 2 h of catalyst 1 using 0.1M nBu4NPF6 as supporting electrolyte in propylene carbonate solution. (D) UV-Vis spectrum of zinc catalyst 1 containing electrocatalysis solution before (black) and after the constant potential electrolysis (red and blue) for 2 h.

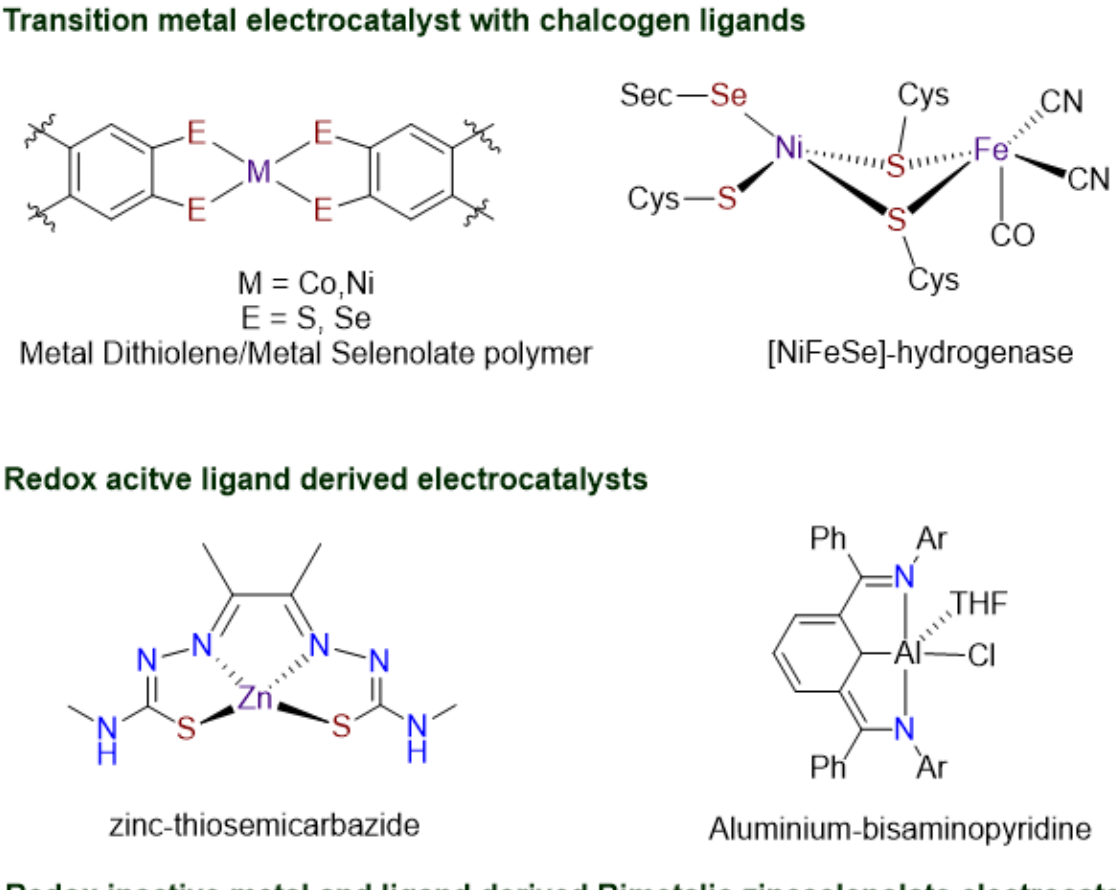

Figure 4

Scheme 1. Chalcogen containing and ligand assisted electrocatalysts for hydrogen and oxygen evolution. Catalyst in the first and second row catalyzes the reduction of protons into hydrogen gas

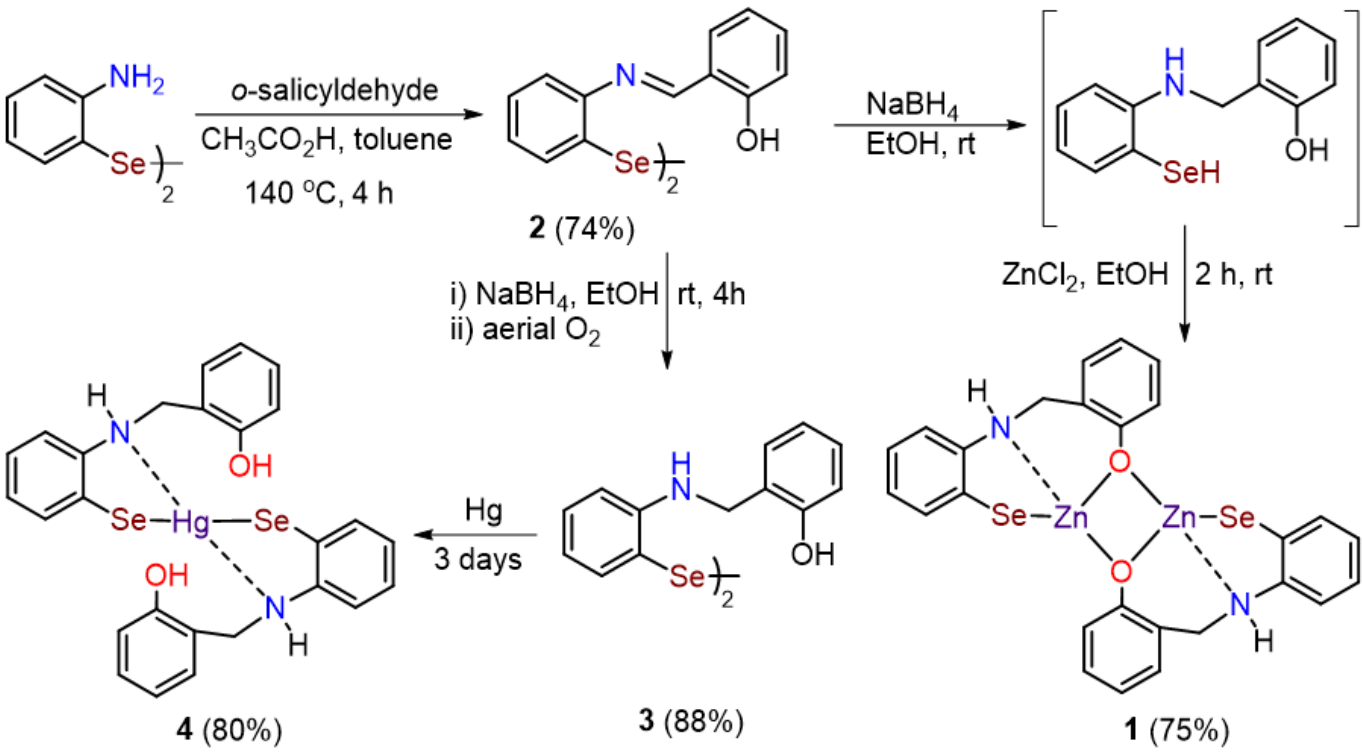

Figure 5

Scheme 2. Synthesis of zinc and mercuric selenolates 1 and 4

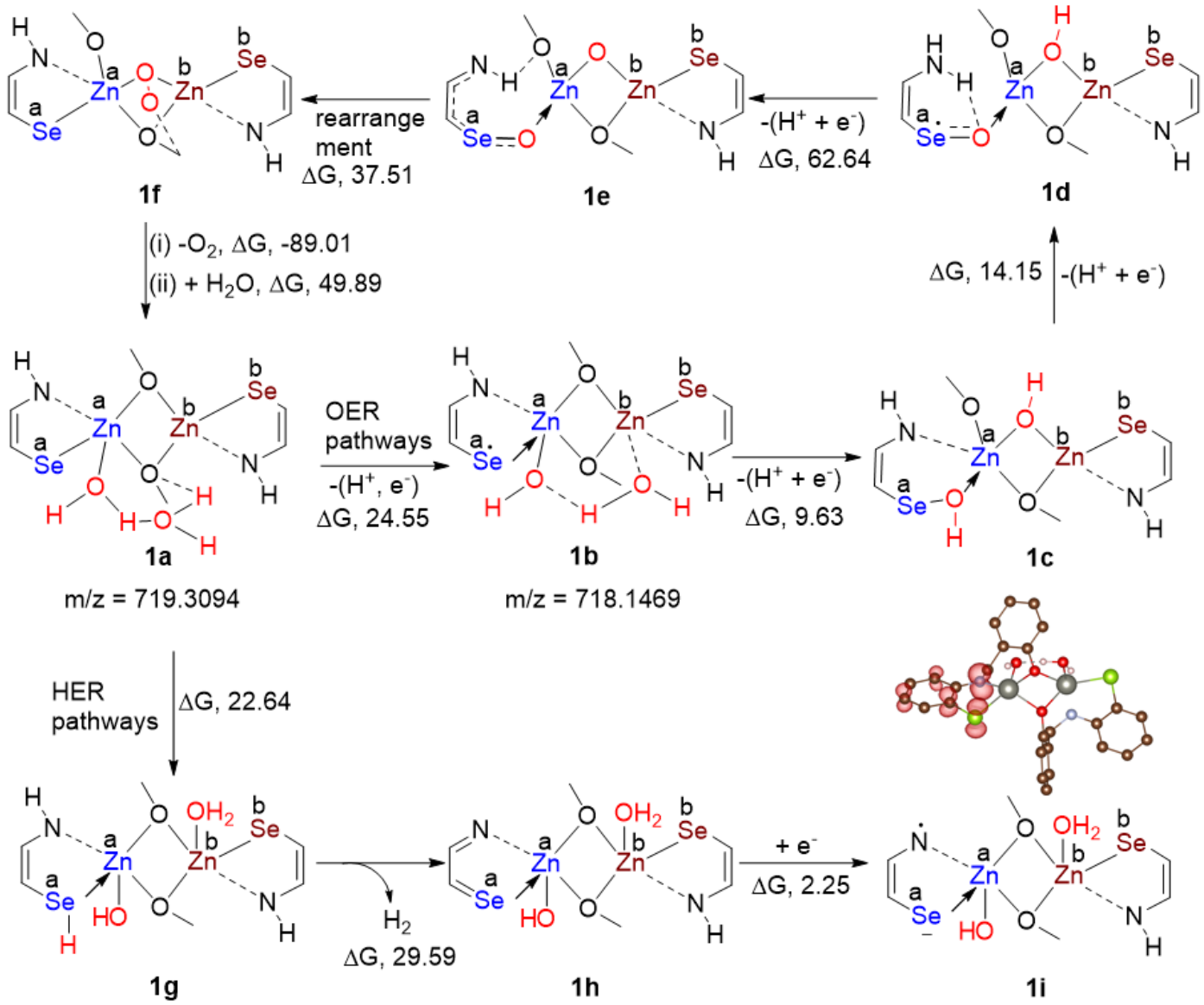

Figure 6

Scheme 3. Mechanistic pathway for OER and HER from water. Only reaction sites of the catalytic intermediates (1a-1i) are shown for clarity. The free energy (in kcal mol-1) has been calculated in B3LYP/def2-TZVP level of theory. The spin density in the inset is plotted at the isosurface value of 0.007 a_0^(-3). Se and Zn atoms are labelled as Se(a), Zn(a), Se(b), and Zn(b) for mechanistic understanding.

Supplementary Files

This is a list of supplementary files associated with this preprint. Click to download.

- SupportingInformation.pdf
- zincselenolate1.cif

- RawData.rar
- Massdataofintermediate1a.rar
- Massdataofintermediate1b.rar